We are IntechOpen, the world's leading publisher of Open Access books Built by scientists, for scientists

4,800
Open access books available

122,000
International authors and editors

135M
Downloads

Our authors are among the

154
Countries delivered to

TOP 1%
most cited scientists

12.2%
Contributors from top 500 universities

CLARIVATE ANALYTICS BOOK CITATION INDEX INDEXED

WEB OF SCIENCE™

Selection of our books indexed in the Book Citation Index in Web of Science™ Core Collection (BKCI)

Interested in publishing with us?
Contact book.department@intechopen.com

Numbers displayed above are based on latest data collected.
For more information visit www.intechopen.com

11

Nano-crystals for quadratic nonlinear imaging: characterization and applications

Sophie Brasselet
Institut Fresnel, Domaine Universitaire St Jérôme, 13397 Marseille Cedex 20 France

Joseph Zyss
Laboratoire de Photonique Quantique et Moléculaire, Institut d'Alembert, ENS Cachan, 61 av. du président Wilson, 94235 Cachan France

1. Introduction

Nonlinear optics is a well established field today, covering a large and rich range of applications which expands every year. Its extension to sub-wavelength scale processes is however highly non trivial, and nano-scale nonlinear optics is only in its infancy. Downscaling high order light-matter optical interaction is however nowadays accessible using new technological tools such as near field techniques, high resolution microscopy and pulsed femtosecond lasers. As a consequence, a large amount of effort has been recently invested into the invention and engineering of nano-structures that exhibit nonlinear optical properties and lead to new optical functions. Among the promising routes followed by nonlinear nano-optics, the development of new nano-sources originating from frequency mixing processes is particularly successful. In this chapter, we describe how nano-crystals have been advantageously developed and used in Second Harmonic Generation (SHG) (or by extension Sum Frequency Generation : SFG), which is the lowest order nonlinear process, dependent on the square of the incident field (Boyd, 1992). Recent developments have shown that these nano-structures are potentially key elements in various fields, such as new nano-probes for bio-imaging, or nano-scale optical fields probing in the ultra-short pulses regime. They also combine the interesting properties of frequency mixing processes with the nano-scale regime: unlike the resonant fluorescence process, coherent harmonic generation is active in the non-resonant regime and therefore free from photo-bleaching which is otherwise generally considered a major drawback from fluorescent nano-probes today. The coherent nature of frequency mixing also allows generating different wavelengths and therefore creating nano-sources of a large range of possible frequencies. An additional advantage of these nano-sources is to avoid phase-matching constraints since their size is well below the coherent length of the underlying nonlinear process, at which nonlinear propagation suffers from destructive interferences between the propagating and induced nonlinear waves. The availability of a large emission frequency range finally allows imaging

bright nano-emitters over a dark background in complex environments sometimes contaminated by auto-fluorescence such as in living cells.
The coherent build up of an induced dipole at twice the frequency of the incident field demands a material exhibiting a non-centrosymmetric structure, which explains why crystals featuring such a structure, although not a majority, have been such determining materials in nonlinear optics to these days, both as a source of inspiration as well as towards applications (Boyd, 1992; Chemla & Zyss, 1987).

As shall be reviewed in the first section of this chapter, downscaling non-centrysymmetry to the nano-scale has been achieved following different possible routes, covering both bottom-up to top-down approaches, in organic as well as in inorganic structures. These nano-probes, which are the nano-scale counterparts of the traditional nonlinear active bulk materials, require specific attention with respect to material engineering. Indeed working at nanometric scales requires revisiting the basic rules of nonlinear optics such as phase matching and nonlinear coupling optimization, which lead to original light-matter interaction processes. Very much like in linear optics, working with nano-objects in nonlinear optics is therefore a research field in itself.
While the study of nonlinear bulk crystals has largely developed along the search for macroscopic nonlinear coupling directions and phase matching conditions, the investigation of nonlinear nano-crystals requires a complete different approach, furthermore constrained by the lack of control of the orientation of the object in the macroscopic framework. In this context, determination of the orientation of the nanocrystal with respect to the laboratory framework sets a problem by itself, thus in considerable contrast with the case of bulk crystals which can be in most cases cut and oriented at will. We will describe in the second section of this chapter the different techniques which have been advantageously developed, either based on a randomization of the nano-crystals orientation in solution, or by immobilization on a substrate by nonlinear microscopy.
Finally, the last section of this chapter will summarize the actual status of applications of nonlinear active nano-crystals, both for bio-imaging using nonlinear microscopy in living cells and tissues, and for nanophotonics, in particular for nano-scale optical fields probing.

2. Nano-crystals development for Second Harmonic Generation

The conception and fabrication of crystals with nanometric to sub-micrometric size exhibiting strong nonlinear quadratic optical responses is a topic of growing interest. In particular, Second Harmonic Generation (SHG) active nano-crystals offer a broad range of potential applications from nanoprobes for bio-imaging to nano-scale photonics with original optical properties. SHG, which provides the ability to transform an exciting optical frequency into its harmonic, when transposed to the nano-scale, could provide new types of light sources and labels with (i) an emission wavelength far away from its excitation (in particular in the infra-red range, which is better adapted to bio-imaging in tissues) (ii) a lower photobleaching probability due to the possibility to work far from resonances, (iii) possibility to tune the emission wavelength by tuning the incident one, or by performing frequency mixing of different excitations, (iv) a less stringent dependence, compared to bulk crystals, on phase matching conditions.

The first prerequisite condition when engineering a SHG-active nano-object is to obtain a non-centrosymmetric structure. As seen in the examples below, a large amount of researches have lead to new routes of fabrications of SHG-active nano-crystals, in order to meet this requirement: either by using crystal unit-cell structures deprived of center of symmetry in inorganics, or engineering a non-centrosymmetric packing of non-centrosymmetric molecules in molecular organic crystals (Chemla & Zyss 1987). As a positive consequence, the coherent emission from SHG-active nano-crystals is supposed to be weakly dependent on the shape of the nano-structure, contrary to metallic nanoparticles which rely on the non-centrosymmetry breaking at their interface. Nevertheless, such shape dependence remains a research topic of interest for nano-objects of the order of a significant fraction of the wavelength (typically from a few ten's to a few hundred's of nanometers). In addition, these structures are expected to exhibit a small size-dispersion, to be amenable to manipulation in solution, and ultimately to be bio-compatible, which imposes low chemical reactivity, low toxicity, stability in aqueous environment, and possibly surface functionalization. They are finally also expected to lend themselves via adequate biomineral or bio-organic linkage, to tethering to some biological material of interest, such as towards the SHG monitoring of intra or inter cellular traffic of a DNA fragment, a biotine-avidine linkage moiety, a protein, an antigen-antibody pair or a deactivated virus. As described in this section, various strategies have been developed to achieve stable and efficient SHG nano-emitters, either from a top-down or from a bottom-up approach.

2.1 Organic nano-crystals

Molecular based nano-crystals are the first structures developed as SHG-active nano-materials. Based on molecular nano-assemblies, they have been designed starting from SHG active asymmetric molecules as individual building blocks, and further grown from a bottom-up approach. The fabrication of these novel nanomaterials constitutes an alternative approach to the synthesis of multichromophoric architectures, which has been a trend over the last decade (Yokoyama et al. 2000, Rekaï et al. 2001, Le Bozec et al. 2001). Molecular-based assemblies present furthermore the advantage of a large flexibility with respect to the nanoparticle nature and the active molecule used. The fabrication procedure follows an essential requirement, which is to conserve the molecular non-centrosymmetry at the nanometric scale, in addition to a high molecular density packing, which ensures SHG efficiency. Assuming indeed a nano-object consisting of n molecules of induced nonlinear dipoles oriented in the same direction, the overall SHG signal is proportional to n^2, which can lead to measurable signals in nanostructure of tens of nanometer sizes (Brasselet & Zyss 2007) (see Section 3).

One of the first reports of second-harmonic emission for nanoscale molecular crystals (Shen et al., 2000) was referring to the emblematic NPP structure (NPP for N-(4-nitrophenyl)-(L)-prolinol)) whereby the usual trend towards centrosymetry had been fought by introduction into the molecular structure of a chiral amino-acid fragment (proline alcool derivative) (Zyss et al. 1984) and which had marked a milestone in nonlinear molecular crystals as the first infrared optical parametric oscillator (Josse et al. 1992). Another early example was based on the non-centrosymmetric CMONS molecule (α-[(4'-methoxyphenyl)methylene]-4-nitro-benzene-acetonitrile, a polar donor– acceptor nonlinear structure) (Figure 1a), from which nano-crystals have been fabricated by rapid nucleation of

the molecules, confined in the nano-pores of a silica network sol-gel (1:1 tetramethoxysilane (TMOS) : methyltrimethoxysilane (MTMOS)) formed by spin-coating (Sanz et al. 2001). The size of the nano-crystals, ranging from 20 to 100nm with a remarkable monodispersity, was controlled by the growth kinetics and parameters such as temperature, matrix porosity, and the CMONS:alkoxides molar fraction (Sanz et al. 2001, Treussart et al. 2003). The study of individual nano-crystals by SHG microscopy has confirmed the non-centrosymmetric structure of the nano-objects, which was consistent with the bulk symmetry (Brasselet et al. 2004). Although these structures showed very efficient SHG activity in addition to two-photon fluorescence, they were embedded in a gel film and therefore not useable for future labelling and manipulation.

Developing isolated nano-objects which can be manipulated in solution has been achieved in $MnPS_3$/DAZOP particles of 10nm size, based on the hybrid bottom-up synthesis of an intercalation compound consisting of push-pull organic chromophores (DAZOP : (4-[2-(4-dimethylaminophenyl)azo]-1-methylpyridinium) embedded in a layered manganese hexathiohypodiphosphate ($MnPS_3$) inorganic host lattice (Yi et al. 2004) (Figure 1b). The DAZOP non-centrosymmetric ferroelectric-like arrangement is obtained within the layered $MnPS_3$ matrix taking advantage of ionic interactions operating during the particle formation within nanoreactors provided by inverse micelles (typically using Brij97 as a surfactant). This strategy has lead to particles with an average second order hyperpolarisability β of the order of 42.10^{-27} esu, measured by Hyper Rayleigh Scattering (HRS) (Yi et al. 2005) (see Section 3). This value is three to four orders of magnitude higher than the β coefficient typically measured in nonlinear molecules. Studies by SHG microscopy (see Section 3) on individual particles immobilized in PVA (polyvinylalcohol) spin coated thin films have shown that the particles tend to form aggregates of larger size (about 100nm), still preserving a quasi one-dimensional order (Delahaye et al. 2006, Delahaye et al. 2009). The stability of the SHG emission from these particles was seen to be strongly dependent on the surfactant used for the synthesis, suggesting an environment dependence of the particle photo-damage (Delahaye et al. 2009).

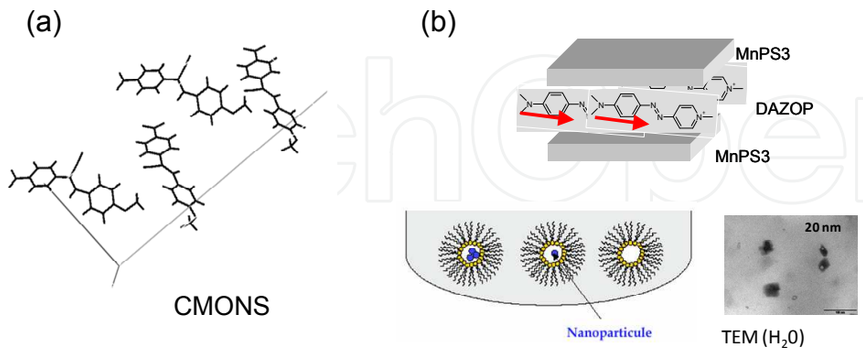

Fig. 1. (a) Unit-cell structure of the CMONS macroscopic crystal in its non-centrosymmetric form. (b) $MnPS_3$/DAZOP nano-crystals : scheme, fabrication procedure and Transmission Electron Microscopy Image.

Top-down approaches have also been attempted to reach molecular nano-crystals. Crystal grinding has been tested on the very efficient co-inclusion compound based on the

confinement of guest non-linear active molecules within the host polycyclic hydrocarbon perhydrotriphenylene (PHTP) channels (Komorowska et al. 2005). The photoactive molecules DANA (4-Dimethylamino-40-nitroazobenzene), used as guest systems, lead to typical bulk values of 340 pm/V. Particles of sizes ranging from 400 to 1000 nm (for which the goal of mono-dispersion had not been pursued at this stage) could be obtained after fine grinding in a PVA-water solution, followed by sonication. Adequate dilution before spin-coating allowed obtaining isolated particle active for SHG and Two Photon Fluorescence.
Another interesting structure, building-up on the concept of octupolar symmetry (Zyss & Ledoux 1994) has been developped based on TTB (1,3,5-tricyano-2,4,6-tris(p-diethylaminostyryl)benzene), a third-order symmetry molecule forming highly efficient nonlinear crystals (Le Floc'h et al. 2005). Micro- and nano-crystals have been investigated (Brasselet & Zyss 2007). 3D Octupolar symmetry evidences in principle an optimized structure whereby the SHG response does not depend neither on the incident polarization nor on the orientation of the object (Brasselet & Zyss 1998). However in the case of TTB, the planar geometry still led to a highly anisotropic nonlinearity (Le Floc'h et al. 2005). Resorting to a fully 3-D octupolar structure (Zyss & Ledoux 1994) would allow generating an orientation independant SHG response, which is of considerable interest for nano-crystal tracking for instance.

Among other possibilities, the fabrication of molecular aggregates from micelles structure based on the mixing of surfactant and active molecules has also been successful to generate non negligible SHG signals (Eisenthal 2006). These structures, which size can be easily engineered, are interesting model systems to study the contribution of surface effects in the nonlinear radiation from sub- micrometric size objects (Revillod et al. 2008).

2.2 Inorganic nano-crystals

While organic nano-crystals can exhibit a wide range of absorption wavelengths governed by chemical synthesis, inorganic nanostructures are often transparent from the visible to 12 μm. A large amount of studies is currently undertaken in order to fabricate robust, transparent, mono-disperse functionalizable inorganic nano-crystals, with typical sizes ranging from 10 to 300 nm. Since the nano-structures described below exhibit very similar nonlinear coefficients (typically in the range 10-30 pm/V in bulk), the goal of the report below is not to discuss their relative efficiencies but rather to give an overview of the fabrication and application routes exploited so far. Efficiency measurement issues are discussed in Section 3 of this chapter.

Zinc Oxide (ZnO) nano-crystals are among the first inorganic nano-crystals studied for nonlinear optics (Johnson et al. 2002). Made of a nontoxic and biocompatible semiconductor material, ZnO nano-crystals were later synthesized in organic media by using a nonhydrolytic sol−gel process and subsequently dispersed in aqueous media using phospholipid micelles, leading to successful encapsulation such as used for drug delivery (Kachynski et al. 2008, Kuo et al. 2009). Further incorporation with the biotargeting molecule folic acid makes this structure adapted to a wide range of targeted bio-imaging studies. ZnO nano-crystals of <100nm size have been synthesized, with additional X-ray diffraction and Transmission Electron Microscopy (TEM) ascertaining for their tetragonal (and pyramid shape) structures (Kachynski et al. 2008). ZnO exits also in the form of nano-wires of typical

1 μm lenths with hexagonal cross-sections, which have been studied also for bio-imaging applications (Nakayama et al. 2007).

The non-toxicity of Iron Iodate has motivated the fabrication of $Fe(IO_3)_3$ nano-crystals of typical size 20-300nm, by co-precipitation synthesis (Galez et al. 2006). The $Fe(IO_3)_3$ material belongs to the hexagonal space group $P6_3$ with nonlinear coefficients in bulk of about 10pm/V off resonance. Nano-crystals of 30 nm sizes have been seen to aggregate in larger clusters (80nm) when the solvent is evaporated on a surface (Bonacina et al. 2007).
Single-crystalline $KNbO_3$ nano-wires of rectangular cross-section of 40nm-400nm x 1-20 μm sizes (depending on the reaction time) could be obtained by a hydrothermal method, mixing at high temperature Potassium hydroxide and niobium pentoxide in deionized water (Magrez et al. 2006). Structural characterizations showed a conserved orthorhombic phase (*mm2*) with the growth axis of the wires parallel to the [011] direction. A rough estimate for the averaged nonlinear coefficient of $KNbO_3$ nano-wires lead to equivalent bulk values of about 10-30 pm/V, as expected in $KNbO_3$ crystals. These $KNbO_3$ nano-wires have been applied to trapping and bio-imaging in living cells (Nakayama et al. 2007).

Aside from these bottom-up techniques, nano-crystals have also been obtained from powders, with a good size dispersion ascertained by Dynamic Light Scattering (DLS) experiments.
$KTiOPO_4$ (KTP) nano-crystals, isolated from a flux-grown powder extracted from a bulk crystal, can be commercially provided (Cristal Laser). These nanocrystals are monodisperse in size (with sizes ranging between 10nm and 80nm). KTP belongs to the orthorhombic point group *mm*2 with typical nonlinear coefficients ranging from 2 to 17 pm/V off resonance. Thorough studies have been undertaken on isolated KTP nano-crystals, in order to measure small size crystals (Le et al. 2006), infer their three-dimensional orientation on substrates (Sandeau et al. 2007), and relate SHG and size information using combined atomic force microscopy and optical techniques (Le et al. 2008).
At last, $BaTiO_3$ nano-crystals of 30nm and 90nm sizes were obtained from commercial dry powders (Nanoamor (30nm) and Techpower (90nm)). Specific studies have allowed a good control of the dillution behavior of the particles in solution to further bio-imaging applications (Hsieh et al. 2009, Hsieh et al. 2010). By dispersion in aminomethylphosphonic acid and sonication of the colloidal solution, the phosphonic acid reacts on the particle surface, ending up with an amine group coating, which introduces an electrostatic repulsion between the particles. $BaTiO_3$ is of tetragonal structure with similar range of nonlinear coefficients as in the crystals reported above. Measured efficiency cross section on single nano-crystals has been evaluated and seen to surpass, by orders of magnitude, the typical fluorescence cross section from traditionally used molecules in two-photon fluorescence (Rodriguez et al. 2009b, Pu et al. 2008, Hsieh et al. 2009).
In all the examples above, considerable stability and efficiency of the measured signals could be observed, as compared to traditional nano-probes used in fluorescence. It is therefore not surprising that many of the previously described structures (ZnO, $Fe(IO_3)_3$, $BaTiO_3$ and $KNbO_3$) have been directly applied to imaging in biological media (see Section 4 of this chapter).

Semi-conductor quantum dots are now the smallest existing structures active for SHG with typical sizes ranging from 2 to 15 nm. While semiconductor quantum dots are widely known and used in fluorescence microscopy as bio-markers, their use for nonlinear

radiation has been much less studied. CdS and CdTe cadmium based materials are both based on a zinc blende crystal structure of cubic Tetrahedral Td symmetry. CdS nanoparticles of about 5 to 10 nm were first synthesized by co-precipitation reaction between an aqueous solutions of $Cd(NO_3)_2$ and Na_2S in the presence of hexametaphosphate (HMP) as a stabilizer (Fu et al. 2001, Wang et al. 2005). Measured hyperpolarizabilities in solution by HRS were found to be up to 7.24×10^{-26} esu, which is four orders of magnitudes higher than typical nonlinear molecules. This value was found to be higher than the one expected from a pure bulk response (typically 78pm/V off resonance), indicating possible surface effects (Fu et al. 2001).
CdTe/CdS nanocrystals with a diameter of 10 to 15 nm have been recently studied by SHG microscopy, immobilized in a PMMA (Polymetylmetacrylate) thin film (Zielinski et al. 2009). Their synthesis is based on a progressive crystalline growth in a noncoordinating solvent, by regular injection of cadmium oleate solution and trioctylphosphine/Te followed by trioctylphosphine/S. Polarization analysis of the second-harmonic emission confirms the expected zinc blende symmetry (see Section 3). The nonlinear efficiency of these structures is expected to come predominantly from the core (with a bulk CdTe nonlinear coefficient of about 150 pm/V), even though the shell is also non-centrosymmetric. In addition to the possibility to observe very small nano-crystals thanks to a high efficiency, intriguing wavelength dependence of the SHG efficiency indicated a probe of deep resonant levels mechanisms (Zielinski et al. 2009).

3. Optical characterization of SHG active nano-crystals

SHG is a multiple field tensorial coupling process, involving both the crystal symmetry and the incident fundamental as well as outgoing harmonic fields polarizations. This coupling has been accounted for by introduction of the nonlinear tensor field and its contraction with the molecular susceptibility tensor, a procedure that can be generalized to any order, leading to a convenient invariant scalar formulation (Boulanger et al. 1997, Brasselet & Zyss 1998). Furthermore, in objects smaller than the focal excitation volumes, the SHG efficiency grows with the object size, as expected from the higher number of active molecules/unit cells (Brasselet 2010). Therefore the analysis of a SHG signal from an isolated object, and in particular the measure of its efficiency, relies on the knowledge of its orientation, its symmetry, and its size relative to the excitation focal volume. While size information can possibly be known on average by techniques such as Dynamic Light Scattering (DLS), Transmission Electron Microscopy (TEM), or Atomic Force Microscopy (AFM), symmetry information can be inferred from bulk structures or more rarely from X-ray diffraction studies on an ensemble of nano-objects. Although these measurements provide averaged information, they can be still valuable as a first input for SHG investigations from single nano-crystals. In particular the nano-crystals symmetry will often be considered to be the same as for the bulk, thus preserved at the nano-scale.

In a planar wave approximation, the overall measured SHG intensity of a single nano-crystal originates from the coherent sum of n induced nonlinear dipoles, n being the number of molecules (or crystalline unit-cells) contained in the nano-crystal present in the focal volume of excitation (Delahaye et al. 2009, Brasselet 2010). The macroscopic components of

these induced nonlinear dipoles, projected in the *(X,Y,Z)* macroscopic frame, are proportional to:

$$P_I^{2\omega}(\Omega) = n\sum_{J,K}\beta_{IJK}(\Omega)E_J^{\omega}E_K^{\omega} \tag{1}$$

with *(I,J,K)* = *(X,Y,Z)*, and $\beta_{IJK}(\Omega)$ being the SHG tensorial component of the crystal unit-cell (or unit molecule) oriented along the Euler set of angles $\Omega = (\theta,\phi,\psi)$. E_J^{ω} is the projection of the incoming field polarization at the ω fundamental frequency on the *J* macroscopic direction. From a microscopic point of view, $\beta_{IJK}(\Omega)$ originates from the projection of the microscopic unit-cell nonlinear hyperpolarizability β_{ijk} *((i,i,k)= (1,2,3)* being the unit cell frame), projected in the macroscopic frame, and can be written (Zyss et al. 1982):

$$\beta_{IJK}(\Omega) = \sum_{i,j,k}\left(\vec{i}.\vec{I}\right)(\Omega)\left(\vec{j}.\vec{J}\right)(\Omega)\left(\vec{k}.\vec{K}\right)(\Omega)\beta_{ijk} \tag{2}$$

with $\left(\vec{i}.\vec{I}\right)(\Omega)$ the cosine projection factor between the*i* (microscopic) and *I* (macroscopic) axes. Note that $d_{ijk} = N\beta_{ijk}/2$ are the traditionally used nonlinear coefficients in a bulk crystal with *N* the molecular (or unit-cell) density. They can therefore be used as known numbers in this expression. Eq. (2) is inferred from the oriented gas model (Zyss et al. 1982), widely used in the understanding of nonlinear responses from organic materials. It assumes in particular that there is no significant interaction between the molecules which therefore behave such as uncorrelated nonlinear emitters, which has been a realistic approach in many examples, subject of course to adequate local field corrections, such as the classical Lorenz-Lorentz or Onsager terms.

As described in the next Sections, two measurements of the macroscopic information from the nonlinear induced dipoles radiation can be performed:

- An incoherent summation over a large collection of n_{nc} nano-crystals, all macroscopic dipoles $P_I^{2\omega}(\Omega)$ being oriented in random directions and positions, from either time or spatial (or both) fluctuations (see Section 3.1). In this case the overall intensity analyzed along the I polarization direction is proportional to:

$$I_I^{2\omega} \propto \left\langle \left|P_I^{2\omega}(\Omega)\right|^2 \right\rangle_{\Omega} = n_{nc}\sum_{J,K} n^2 \left\langle \beta_{IJK}(\Omega)\beta_{ILM}(\Omega)\right\rangle_{\Omega} E_J^{\omega}E_K^{\omega}E_L^{\omega^*}E_M^{\omega^*} \propto n_{nc}.n^2.\left\langle\beta^2\right\rangle.\left(I^{\omega}\right)^2 \tag{3}$$

  With $\sqrt{\left\langle\beta^2\right\rangle}$ being the averaged measured nonlinear coefficient. The incoherent nature of the process imposes in this case that the signal is proportional to n_{nc}, the number of nano-crystals in the focal volume.

- A direct coherent measurement of the macroscopic radiating dipole $P_I^{2\omega}(\Omega)$ from a single nano-crystal oriented in the Ω direction (see section 3.2):

$$I_I^{2\omega}(\Omega) \propto \left|P_I^{2\omega}(\Omega)\right|^2 = \left|n\sum_{J,K}\beta_{IJK}(\Omega)E_J^{\omega}E_K^{\omega}\right|^2 \propto n^2.\beta^2.\left(I^{\omega}\right)^2 \quad (4)$$

In both cases the signal is proportional to n^2 , with n the number of unit-cells (or molecules) in the nano-crystal. Since $n = N.V$ with V the nano-crystal volume and N the crystal density, the measured signals are proportional to the sixth power of the nano-crystal diameter. Note that rigorously, V is the overlap between the excitation volume and the nano-crystal volume itself.

3.1 Averaging SHG information

In order to measure SHG efficiency from nano-crystals while circumventing the issue of their orientation knowledge, studies have been performed using orientation-averaging techniques. Averaging SHG information is typically performed in a powder measurement, which is an historical way to analyse SHG efficiency from molecular micro-crystals (Kurtz et al. 1968, Halbout et al. 1984). Powder analyzes have been performed for instance on ferroelectric Strontium barium niobate nanoparticles of 40 nm size, made from $Sr_xBa_{1-x}Nb_2O_6$ (SBN) (Rodriguez et al. 2009). The drawback of this technique is the lack of knowledge on the possible formation of macroscopic clusters.

Another traditional technique, Hyper Rayleigh scattering (HRS) (Terhune et al. 1965), relies on the measurement of the nonlinear scattering of the nano-objects in solution, which is more amenable to environments where the nano-crystals can be isolated from their neighbours by electrostatic repulsion. HRS, which has been a determining tool for molecular engineering in nonlinear optics (Zyss & Ledoux 1994) including molecular based nano-objects (Le Bozec et al. 2001), is a robust technique to infer averaged nonlinear coefficients from nano-crystals, using known solvents as references. Since the obtained signal is a result of time, spatial and orientational averaging over fast diffusing molecules or particles, this method does not require a preliminary orientation of molecules or particles before study. It has been applied to CdS particles (Fu et al. 2001, Wang et al. 2005), molecular aggregates (Eisenthal et al. 2006, Revillod et al. 2008), hybrid nanoparticles (Yi et al. 2005), $BaTiO_3$ and $PbTiO_3$ nano-crystals (Rodriguez et al. 2009b), and more recently $FeTiO_3$ nano-crystals (Mugnier et al. Submitted). $\sqrt{\langle\beta^2\rangle}$ averaged coefficients up to more than 10^{-26} esu have been measured, which is orders of magnitudes above single nonlinear molecules, due to their size extension into larger scale aggregates (as a comparison a DAZOP molecule efficiency is typically 220.10^{-30} esu (Yi et al. 2005)).

While these techniques are powerful to provide an averaged efficiency estimation of nano-crystals, they are however strongly limited when analysis is needed at the single nano-object level, which is the relevant one towards nano-crystal engineering. In particular, no particular knowledge can be inferred on the crystalline quality of isolated crystals, neither on their possible behaviour distributions.

3.2 SHG imaging of single nano-crystals

SHG microscopy, initially introduced as an imaging tool to visualize the microscopic crystal structure in polycrystalline ZnSe (Hellwarth, 1974), allows today investigating nano-crystals one by one, provided they are sufficiently distant from one another (typically by 1 μm) on a glass substrate or in a polymer thin film. SHG microscopy is based on the illumination of a

nano-object by focussing the light of a pulsed laser (for instance a Ti:Sa laser, tuneable between 690 nm and 1050 nm (150fs pulse width, 80MHz repetition rate), using a high numerical aperture objective (NA ranging between 0.9 and 1.4). The focused light forms a focal volume of typically 300 nm in the lateral dimension and 700 nm in the axial direction. In a typical SHG microscope, the SHG emission from nano-objects is collected backward through the same objective as used for the fundamental excitation, then filtered-out spectrally to possibly remove remaining laser light and fluorescence emission, and focused on avalanche photodiodes (Figure 2a). The final image of nano-crystals is generally obtained by scanning either the sample on a piezoelectric mount or the excitation beam by galvanometric scanners, over typically 20 μm to 100 μm dimensions (Figure 2a) (Brasselet et al. 2004, Brasselet & Zyss 2007). Other implementations have been performed based on the phase information from the SHG signal in single nano-crystals, taking advantage of the coherent nature of this optical process. Based on interferometric measurements with a reference signal coming from the SHG field of a macroscopic nonlinear crystal, these implementations have allowed either a direct phase measurement in a homodyne detection set-up (Figure 2b, Le et al. 2006), or 3D imaging using digital holographic image reconstruction (Figure 2c, Pu et al. 2008). The first scheme has allowed measuring KTP nano-crystals below 30nm size, benefiting from the homodyne detection sensitivity provided by the local oscillator (Le et al. 2006). The second provides a scheme for a scan-free 3D imaging. In this case sensitive CCD camera is placed away from the object plane, and the image is added coherently with a reference SHG plane wave. By digital propagation in the observed interference pattern, the field is reconstructed at any plane, with a diffraction limited resolution (Pu et al. 2008).

In the context of quadratic nonlinear microscopy, let us also mention a parent technique, also resorting to a frequency mixing process, the Pockels linear electro-optic effect that is leading to an $\omega \pm \Omega$ optical frequency modulation, where ω and Ω stand respectively for the higher frequency of the illuminating optical laser field and for the lower one attached to an externally applied electric voltage (herein ranging from the kHz to a few tens of MHz). In an interferometric read-out configuration using a sensitive homodyne detection to boost the modulated signal while minimizing the intensity actually shining the material, this configuration turns out to be compatible with low cw power (typically 100μW). This effect has been implemented and applied to poled polymers (Toury et al. 2006), doped artificial membranes (Hajj et al. 2009), and more recently to KTP nano-crystals down to 100 nm size (Hajj et al. Submitted).

Obviously a SHG image of many isolated nano-crystals exhibits a wide range of intensities (Figure 2a), for several reasons:

- This is first due to the size variations between nano-crystals, their efficiency scaling with the sixth power of their diameter, as detailed above. In addition an estimation of size variations in the 10-100 nm range is impossible: any size below the diffraction limit exhibits an image spot of roughly 300 nm size, and only crystals sizes above this limit can be discriminated.
- Even in a mono-disperse population, intensity variations occur from the wide range of possible orientations of nano-crystals in the sample, coupling with different efficiencies to the incident polarization as seen in Eq. (4).

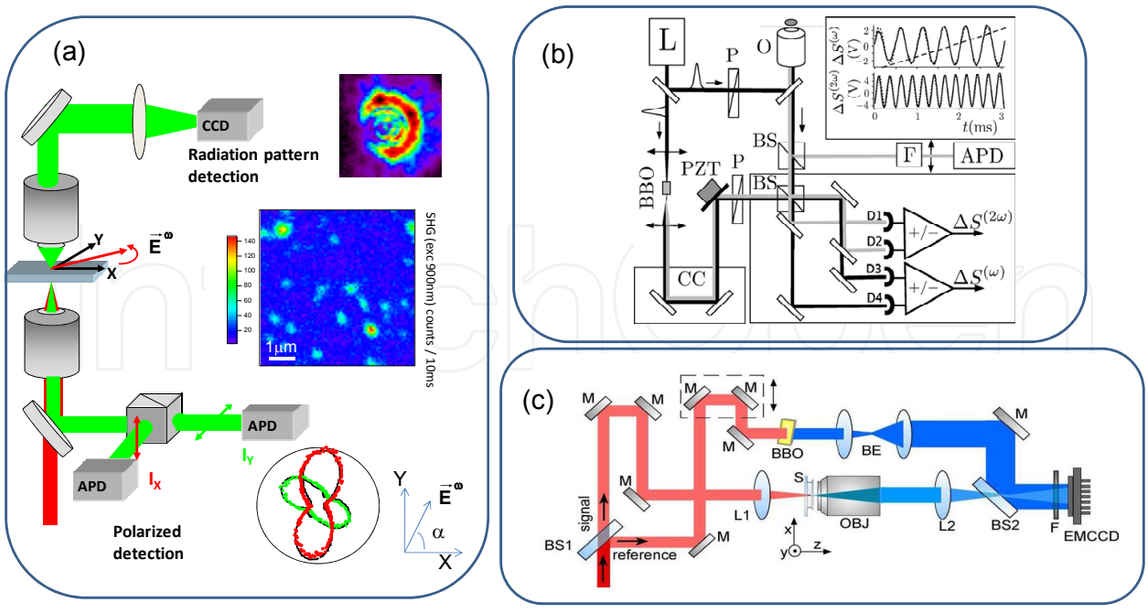

Fig. 2. (a) Imaging and polarization resolved nonlinear microscope. A polarizing beamsplitter separates the signal towards two avalanche photodiodes (APD). SHG polarimetry consists in recording the SHG emission while the incident linear polarization is rotated (angle α) on two orthogonal analysis directions (I_X and I_Y are represented in polar plots in red and green respectively for a given nano-crystal). A typical SHG image (from Brasselet 2010) is shown from a thin PVA polymer film containing MnPS3 particles ($MnPS_3$/DAZOP/Brij97, 10^{-4} mol/L DAZOP). Excitation wavelength : 920nm (a SHG spectral filter is placed in the detection path at 460 nm - excitation power: 1 mW-SHG signal scale : counts/50ms). A defocused imaging (above) is shown from a 80 nm size nano-KTP (Sandeau et al. 2007). (b) (from Le et al. 2006) SHG balanced homodyne detection set-up. (c) (from Hsieh et al. 2009) Harmonic Holography set-up. On both cases, a reference arm is created by SHG in a BBO (β-barium borate) crystal. While the homodyne set-up restores the information from interferences fringes observed by modulating a mirror position in the interferometer, the holography set-up images directly the phase information in a wide field interference pattern, which is used for further reconstruction imaging.

3.3 Determining orientation and crystallinity information from a single nano-crystal

Measuring a single nano-crystal nonlinear efficiency is therefore not direct and requires careful investigation of the SHG response. In order to approach this issue, knowledge of the SHG polarization coupling mechanism in the nano-crystals is required. In addition to SHG imaging, a full polarimetric analysis has been therefore developed based on the recording of the SHG emission signal under a continuous rotation of the incident linear polarization in the sample plane (Brasselet et al. 2004). The polarization rotation is performed by an achromatic half-wave plate mounted on a rotating step motor, while the signal is recorded on two polarization directions, using two avalanche photodiodes separated by a polarizing beamsplitter (Figure 2a). The orientation (Ω) and symmetry (β tensor) information in the nano-crystal are contained in the $\beta_{IJK}(\Omega)$ coefficients of Eqs. (2) and (4). The principle of polarization-resolved SHG is to tune the field contributions E_J^{ω} by rotating a linear

polarization in the *(X,Y)* sample plane (Figure 2a). Typical polarization responses projected on the *X* and *Y* directions are illustrated in Figure 2a and Figure 3 on a 1D symmetry nano-crystal. Very anisotropic polarization responses can be observed in the direction of the nano-object, as expected, whereas a symmetry containing different orientations, such as in a 1D nano-object cluster, would lead to more complex polarimetric response (Figure 3b).
It is therefore possible, providing that the nano-crystal symmetry or orientation is known, to discriminate mono-crystalline structures from non-crystalline ones (Brasselet et al. 2004, Komorowska et al. 2005, Brasselet & Zyss 2007, Brasselet 2010). A non-crystalline structure is seen in this case as a collection of nonlinear dipoles oriented in different Ω directions adding up incoherently. This information, which is not accessible from an ensemble measurement, is of paramount importance towards further nano-crystals synthesis. SHG polarimetry has been successful in investigating molecular ordered materials (Le Floc'h et al. 2003, Anceau et al. 2005). Recently, demonstrations have shown its potential to provide orientational and structural behaviour of single isolated CMONS nano-crystals (Brasselet et al. 2004), as well as hybrid (Delahaye et al. 2006, Delahaye et al. 2009) and inorganic (Zielinski et al. 2009) nano-crystals.

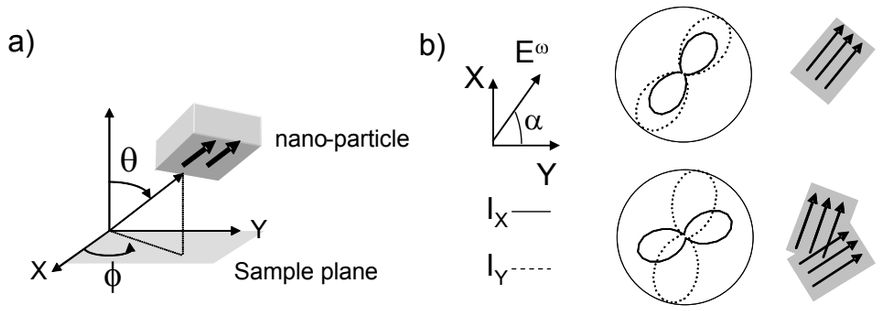

Fig. 3. (a) Representation of the Euler set of angles Ω (θ,ϕ,ψ) defining the orientation of a nano-crystal of high symmetry axis designated by the black arrows. In the case of a nano-object abiding to cylindrical (or higher) symmetry as here, one needs only two Euler angles, the third ψ rotation around the symmetry axis of the nano-object being then unnecessary. (b) Polarization-resolved SHG response from a single 1D symmetry nano-crystal (above) versus a collection of different orientations of 1D symmetry nano-crystals (below). The polarization response is represented as a polar graph in the projection sample plane (X,Y), projected along the X and Y polarization analysis directions.
Several observations must be added to the polarimetric analysis discussed above, including considerations which are crucial towards a proper analysis of polarization dependent SHG data from single nanocrystals.

- *Instrumentation distortions by reflection optics*. In most of the measurements a polarization analysis requires rotating a linear polarization before reflection on a dichroic mirror or other mirrors (Le Floc'h et al. 2003; Chou et al. 2008; Schön et al. 2008). It is know that these optics, although often corrected for a reliable *s/p* (or *X/Y*) intensity reflection ratio, can strongly distort any intermediate polarization angle by applying a phase shift between the *X* and *Y* components. The input polarization, becoming elliptic, needs to be correctly accounted for in the analysis of Eq. (4). This can be done by preliminary calibrations (Le Floc'h et al. 2003, Schön et al. 2008).

- *Effect of the high aperture excitation/collection*. Eq. (4) is written in the plane wave approximation. Observation of single nano-crystal however requires high numerical aperture (NA) objectives for both the excitation and collection of the SHG radiation which requires a more rigorous analysis. Indeed, under such conditions, an incident field polarization in the *(X,Y)* plane is known to contain also *Z* contributions in the focal plane, that can reach up to 45% of the incident amplitude at the edge of the focussing spot (Richards & Wolf 1959). Depending on the nano-crystal off-plane orientation, the SHG signal therefore also contains *Z*-coupling nonlinear coefficient contributions that can strongly alter its polarization response (Yew & Sheppard 2006, Schön et al. 2010). Such contributions are however located spatially at the border of the incoming Gaussian field amplitude, and may induce extra nonlinear coupling terms only for objects reaching 100 nm to 150 nm size. The high aperture collection also mixes-up polarization states of the emission radiation. Both effects can be fully taken into account by a complete model calculating the nonlinear induced dipole at every point of an object placed at the center of the focal spot of the objective (Sandeau et al. 2007, Schön et al. 2010). In general nano-crystals of sizes well below 100 nm will only experience slight modifications of their polarization responses under high NA conditions.

- *Effect of the spatial extension of the nano-crystal*. Another limitation to Eq. (4) is that it considers that the coherently added dipoles are all positioned spatially on the optical axis of the microscope objective, thus ignoring possible phase retardation effects in the volume of the object. Extensive studies accounting for the spatial extension, of a nano-crystal, have shown that for sizes above a few tens of nm, the radiation does not resemble that of a single macroscopic dipole volume (Sandeau et al. 2007), in particular the backward emission is considerably reduced comparing to the forward emission, and phase matching conditions have been re-written accounting for the Gouy phase shift occurring in the excitation volume (Sandeau et al. 2007). Whereas the "punctual object" assumption might be crucial for efficiency measurements in nano-objects of unknown size distribution, it does not however alter the polarization resolved microscopy analyses which are relative measurements.

- *Limitation to a 2D projection information*. The information provided by polarimetric SHG is limited to the projection of the nonlinear tensor in the sample plane *(X,Y)* and is therefore not a complete 3D information. Indeed the excitation field is defined in this plane, therefore only *X* or *Y* coupling directions are allowed in this geometry, except from high NA focusing effects as discussed above. Any information related to off-plane coupling requires complementary analysis. In some cases, as demonstrated for CMONS (Figure 4a), two-photon fluorescence can provide additional information which, combined with SHG, is sufficient to deduce such 3D orientation and crystallinity information from the nano-object (Brasselet et al. 2004). Pure 2D projection analysis in SHG may also lead to the missing 3D information in nano-crystals of complex symmetry involving non-diagonal coupling directions (Zielinski et al. 2009, Brasselet 2010). Another method has been proposed to deduce 3D information from nano-crystals, based on the defocused imaging of the nonlinear radiation from the nano-object (Figure 2a, 4b). This has lead to successful determination of 3D orientation information based on the image analysis of the projection of the nonlinear dipole radiation expansion in the *(X,Y)* sample plane (Sandeau et al. 2007).

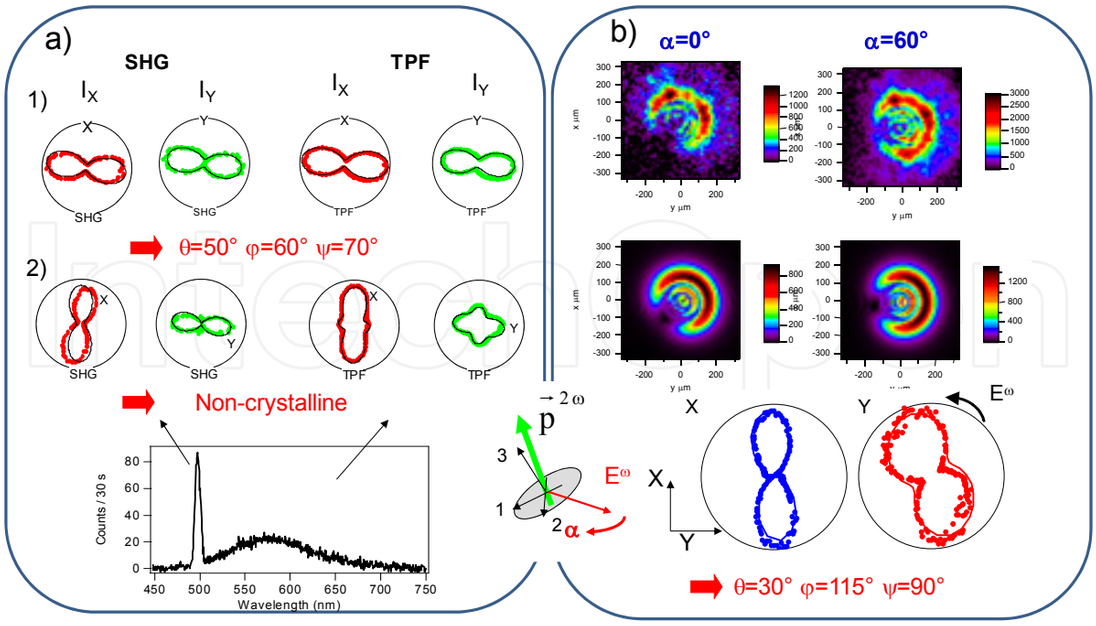

Fig. 4. (a) SHG and two-photon fluorescence (TPF) polarization dependence from two different CMONS nano-crystals embedded in a sol-gel film (Brasselet et al. 2004). The SHG and TPF emission wavelengths can be discriminated and therefore lead to a separated polarization analysis of the two signals. 1) : mono-crystalline nanoparticle which projection in the sample plane resembles that of a 1D nano-object. The 3D orientation of the nano-crystal could be deduced from the simultaneous fit of the X and Y projections of the SHG and TPF responses. 2) typical nano-crystal which polarization response cannot be fit by a pure mono-crystalline orientation. (b) Defocused imaging of 80 nm a KTP nano-crystal for two different input polarizations in the sample plane (α angles). The defocused images, compared to modelling accounting for the full propagation of nonlinear induced dipoles in the microscope, allowed retrieving a 3D orientation information, confirmed by polarimetry (Sandeau et al. 2007).

3.4 Determining the nonlinear efficiency from a nano-crystal

Based on Eq. (4) and assuming that the nano-crystal symmetry and 3D orientation are known, it is now possible to determine its nonlinear efficiency. This is generally done by measuring a reference nonlinear response, similarly as in HRS (Yi et al. 2005, Revillod et al. 2008), which is provided here by a macroscopic crystal. In known excitation/detection polarization coupling directions, the SHG signal from a crystal of known orientation is:

$$I_{ref}^{2\omega} \propto \left(\chi_{ref}^{(2)}\right)^2 .\left(I^{\omega}\right)^2 \tag{5}$$

which nonlinear coefficient $\chi_{ref}^{(2)}$ is taken as a reference. The proportionality coefficient contains the same collection and scaling factors as in Eq. (4), therefore SHG intensities can directly be compared, for a same input power, and a given (IJK) set of polarization conditions:

$$n^2 .\beta_{IJK}(\Omega)^2 = \chi_{IJK}^{(2)}(\Omega)^2 = \chi_{ref}^{(2)} . I_{ref}^{2\omega} / I_I^{2\omega}(\Omega) \tag{6}$$

The macroscopic nonlinear coefficients from a nano-crystal $\chi^{(2)}_{IJK}(\Omega)$ can therefore be measured for a given orientation. Note that this macroscopic coefficient is generated from an object of much smaller size than that of a bulk crystal. Since $\chi^{(2)}_{IJK}(\Omega)$ is proportional to the volume of the nano-object (Eq. (4)), and similarly $\chi^{(2)}_{ref}$ is proportional to the excitation volume V_{exc} in the microscope, the nano-crystal efficiency can be transformed into an "equivalent bulk" value which is the efficiency that the nano-crystal would exhibit if it were filling the whole focal volume: $\chi^{(2)}_{IJK,bulk}(\Omega) = \chi^{(2)}_{IJK}(\Omega).V_{exc}/V$. Typically V_{exc} ~ 60.10^6 nm^3, and V ranges between 10^3 nm^3 and 10^6 nm^3. Note that since the excitation takes place over about 300 nm in the sample plane, it is considered here as homogeneous over the nano-crystal size. More refinements are necessary when the nano-crystal size approaches the diffraction limit size (Delahaye et al. 2009). Values up to 1pm/V have been measured in 100 nm size aligned nano-clusters of $MnPS_3$/DAZOP hybrid nanoparticles, which reach up to 1000 pm/V in an equivalent bulk crystal (Delahaye et al. 2009). In addition of being stable, these nano-crystals are therefore very bright nano-sources.

3.5 Retrieving size information from a nano-crystal

Assuming that both the orientation Ω and efficiency $\chi^{(2)}_{IJK}(\Omega)$ of the nano-crystal can be measured, it is now possible to retrieve size information from this object. For this, the macroscopic to microscopic relation expressed in Eq. (2) is used and introduced in:

$$V = \chi^{(2)}_{IJK}(\Omega)/(N.\beta_{IJK}(\Omega)) \tag{7}$$

Where $\beta_{IJK}(\Omega)$ are deduced from the microscopic nonlinear coefficients β_{ijk} (Eq. (2)), known from the unit-cells crystals values: $d_{ijk} = N\beta_{ijk}/2$ and assuming that both bulk nonlinear efficiencies and density are the same as in the bulk crystal.

Such an analysis has been performed on a large collection of $MnPS_3$/DAZOP hybrid nano-crystals immobilized in PVA (Figure 5), which efficiency were used to evaluate a lower limit to the particles size distribution (Delahaye et al. 2009). The lower limit size given here is imposed by the lack of knowledge of the 3D off plane orientation angle of the nano-crystals (even though the 2D orientation of the dipoles in the plane could be determined by SHG polarimetry as described in the previous Section). The population of the deduced sizes was seen to be consistent with the sizes of the spots measured on the SHG scans, which most often were above the diffraction limit. This analysis allowed in particular evidencing an aggregation behaviour of the nano-particles in the polymer film, which lead to 100 nm size objects. Such statistical analysis, accounting for both SHG polarization dependence and image size measurements, can therefore provide a complete picture of the structural behaviour of nano-crystals.

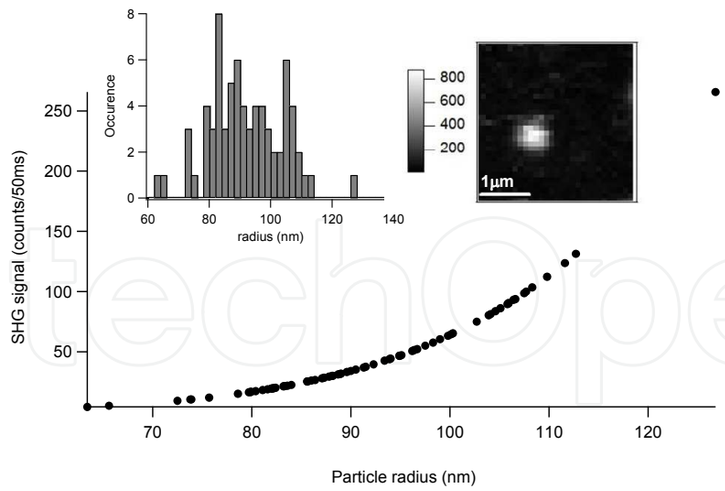

Fig. 5. Histograms of sizes of (MnPS3/DAZOP/Brij97, 10^{-4} mol/L DAZOP) nano-crystals in a PVA polymer film. These sizes were deduced from the SHG signal dependence on the particle radius R (as detailed in the text), depicted in the curve where each marker represents an isolated nano-crystal. In this analysis the DAZOP molecules were assumed to have the same hyperpolarizabtility as in solution, namely $\beta = 220 \times 10^{-30} esu$. The estimated size could be compared to the size measured for each nano-crystal on a SHG scan, which some times surpasses the diffraction limit (Delahaye et al. 2009).

4. Applications

4.1 Bio-imaging

While SHG microscopy, together with polarimetric analyses, is today particularly successful for bio-imaging benefiting from intrinsic responses from bio-molecular assemblies (Campagnola et al. 2002, Zipfel et al. 2003, Stoller et al. 2002, Strupler et al. 2007), biological applications still require efficient nano-emitters that can report biological relevant information at nano-scale in targeted regions of a sample of interest. Several issues such as toxicity, photo-bleaching, instability, lack of sharp contrast, are still considered as strong drawbacks for the fluorescence process which is more traditionally used in bio-imaging.

These issues can be advantageously circumvented by the use of SHG active bio-marker. SHG active nano-crystals are interesting alternatives due to the stability of their emission, the flexibility in the emission wavelengths and the subsequent possibility to observe them over a dark background, and at last their potential to no-toxicity. They can be additionally excited in the IR (700-1500nm), within wavelength ranges that are less scattered by biological media. They also do not exhibit phase-matching constraints contrary to more bulky media, being therefore able to efficiently emit SHG regardless of the phase properties of the excitation field.

ZnO nano-crystals have been successfully used for bio-imaging applications (Kachynski et al. 2008). Sum frequency, second harmonic, and non-resonant four wave mixing nonlinear signals have been obtained from stable dispersion of ZnO nanoparticles targeted to live tumor (KB) cells. Robust intracellular accumulation of the targeted (FA incorporated) ZnO nanocrystals could be observed without any indication of cytotoxicity. A water dispersion of well-separated single nanocrystals was obtained from an encapsulation technique, using

phospholipid micelles formed by the self-assembly of polymer-grafted lipids (Kachynski et al. 2008).
The holographic SHG imaging described in Section 3 allowed 3D imaging of $BaTiO_3$ particles of 30 nm size in HeLa cells, treated by incubation at 37°C with the particles uptaken by endocytosis (Hsieh et al. 2009). The particles were seen to be randomly distributed in the cells, possibly as clusters, into vesicles. The cells were seen to be alive after incubation, and fixed for imaging (Hsieh et al. 2009, Kuo et al. 2009, Hsieh et al. 2010).
At last, $KNbO_3$ was successfully incorporated and optically trapped for imaging in living cells (Nakayama et al. 2007).

SHG active nano-crystals are also of interest as punctual nano-sources for imaging through thick tissues, since the wide range of usable wavelengths can be extended to the IR, which is less scattered by natural media (Bohren & Huffmann, 1983). The wide frequency range available from SHG active nano-crystals has been exploited using $Fe(IO_3)_3$ nanoparticles illuminated at 800nm and 1550nm, in tissue phantoms made of submicrometric polystyrene beads, as well as in a section of a fixed mouse liver (Exterman et al. 2009). Using long working distance objectives (with lower NA objectives down to 0.6), better imaging quality was observed at large depths (180 μm in a phantom) for the larger IR wavelength.
At extensive depths, biological tissues are known to exhibit scattering properties which can also alter considerably the quality of optical focusing. SHG efficiencies can therefore be largely decreased by scattering when exploring large depths. A possible method to correct for the deformation of the optical wavefront brought by the medium is based on phase conjugation, which however requires a point source inside the medium. Indeed in this technique a source is used as a reporter of the local phase of the excitation field; its scattered field is then recorded in amplitude and phase in a hologram, and a phase-conjugated beam, reconstructed from this field, is sent back into the sample, thus providing automatic correction of phase distortions. SHG active nano-crystals (300 nm size $BaTiO_3$) have been used to play the role of the point source (Hsieh et al. 2010). This approach has shown successful digital phase conjugation in turbid media using off-axis digital holography to record the scattered SHG field from the nano-crsytals in a turbid medium made of a layer of parafilm fixed on the particles sample. The measured phase conjugated beam was generated in a spatial light modulator, and then sent back through the turbid medium. This observation of a nearly ideal focus on a nano-crystal, would not have been feasible in linear optics where all possible structures scatter the incident field without any spatial discrimination (Hsieh et al. 2010).

4.2 Nano-scale optical fields probing

The nonlinear mechanism taking place in SHG couples coherently the emission induced dipole to the excitation fields, therefore providing a possible way to probe excitation fields at the nano-scale in phase, polarization and amplitude. Thanks to their sizes, nano-crystals are unique reporters of optical fields properties at nano-scales. This approach has been advantageously used to apply Frequency Resolved Optical Gating (FROG) (Trebino et al. 1997) in single $Fe(IO_3)_3$ nano-crystals under ultra-short excitation (69 fs), bringing new prospective to monitor the phase and amplitude spectral distortions of such pulses (Exterman et al. 2008). This technique, usually performed on bulk samples, is a unique

demonstration that opens to the exploration of optical fields time properties at any place in a focal spot, since the size of the used particle is well below the optical resolution. The additional advantage of the use of nano-crystal is the absence of constraints imposed by nonlinear phase-matching in bulk crystals, which can be limiting in the case of extreme ultra-short pulses analysis.
SHG responses under ultra-short pulses are generally strongly dependent on the spectral and time phase profile of the pulses. In particular the optimum efficiency is reached for Transform Limited pulses, which exhibit no spectral/time dependence in phase over their whole bandwidth ("flat phase"). In order to maximize the SHG response from nano-crystals under short pulses excitations (13 fs to 200 fs), an optimization of the signal has been performed in KTP nano-crystals by directly adapting adequate optimization generic algorithms (Baumert et al. 1997) to their emission signals (Wnuk et al. 2009). As expected, an increase of the emission intensity has been observed when decreasing the duration of the excitation fs pulses.

5. Conclusion

This chapter has given an overview of the current state of research on SHG active nano-crystals. While this field is still in constant progress, many achievements have already allowed revisiting nonlinear optics in order to adapt to the scale of these new nano-objects. Their applications to both nanophotonics and biophotonics fields have shown their potential and are probably only at their infancy.

6. Acknowledgements

We thank Véronique Le Floc'h, Kasia Komorowska, Christelle Anceau, Nicolas Sandeau, Dominique Chauvat, Jean-François Roch, and Isabelle Ledoux for fruitful discussions and contribution to nonlinear microscopy developments in Laboratoire de Photonique Quantique et Moléculaire, ENS Cachan, France. Part of this work has been undertaken in collaboration with Alain Ibanez (Institut Néel, Grenoble, France), Emilie Delahaye and René Clément (Laboratoire de Chimie Inorganique, Institut de Chimie Moléculaire et des Matériaux d'Orsay, Université Paris XI, Orsay, France), S. Perruchas, C. Tard and T. Gacoin (Laboratoire de Physique de la Matière Condensée, Ecole Polytechnique, Palaiseau, France).

7. References

Anceau C., Brasselet S., Zyss J. (2005). Local orientational distribution of molecular monolayers probed by nonlinear microscopy. *Chem. Phys. Lett.* 411(1-3), 98-102

Baumert T., Brixner T., Seyfried V., Strehle M. et Gerber G. (1997). Femtosecond pulse shaping by an evolutionary algorithm with feedback. *Appl. Phys. B: Lasers and Optics*, 65, 6

Bohren C. F., and Huffmann D. R. (1983). *Absorption and Scattering by Small Particles*. Wiley Science paperback, Wiley & Sons, New York

Bonacina L., Mugnier Y., Courvoisier F., Le Dantec R. , Extermann J., Galez C., Boutou V., Wolf J.P. (2007). Polar Fe(IO3)3 nanocrystals as local probes for nonlinear microscopy. *Applied Physics B, Lasers and Optics*, 87(3), 399-403

Boulanger B. and Zyss J. (1997). *Physical Properties of Crystals, Vol. D of International Tables for Crystallography*, A. Authier, ed. Kluwer, Dordrecht, The Netherlands

Boyd R. W. (1992). *Nonlinear Optics*. Academic, New York

Brasselet S. and Zyss J. (1998). Multipolar molecules and multipolar fields: probing and controlling the the tensorial nature of nonlinear molecular media. *J.Opt.Soc.Am.B* 15(1), 257-288

Brasselet S. and Zyss J. (2007). Nonlinear polarimetry of molecular crystals down to the nanoscale. *C. R. Physique* 8, 165-179

Brasselet S. (2010). Second Harmonic Generation microscopy in molecular crystalline nano-objects. *Nonlinear Optics, Quantum Optics* 40 (1-4), 83-94

Brasselet S., Le Floc'h V., Treussart F., Roch J. F., Zyss J., Botzung-Appert E., and Ibanez A. (2004). In situ diagnostics of the crystalline nature of single organic nanocrystals by nonlinear microscopy. *Phys. Rev. Lett*. 92(20), 4

Chemla D.S. and Zyss J. (Eds.) (1987) *Nonlinear Optical Properties of Organic Molecules and Crystals* (Vol.1). Academic Press, Orlando

Chou C.-K., Chen W.-L., Fwu P. T., Lin S.-J., Lee H.-S., and Dong C.-Y. (2008). Polarization ellipticity compensation in polarization second-harmonic generation microscopy without specimen rotation. *J. Biomed. Opt*. 13(1), 014005

Delahaye E., Sandeau N., Tao Y., Brasselet S., Clément R. (2009). Synthesis and Second Harmonic Generation microscopy of nonlinear optical efficient hybrids nanoparticles embedded in polymer films. Evidence for Intra and Inter nanoparticles orientational synergy. *J. Phys. Chem. C,* 113 (21) 9092–9100

Delahaye E., Tancrez N., Yi T., Ledoux I., Zyss J., Brasselet S., and Clement R. (2006). Second harmonic generation from individual hybrid MnPS3-based nanoparticles investigated by nonlinear microscopy. *Chem, Phys. Lett*. 429, 533–537

Eisenthal Kenneth B. (2006). Second Harmonic Spectroscopy of Aqueous Nano- and Microparticle Interfaces. *Chem. Rev.* 106, 1462-1477

Extermann J., Bonacina L., Courvoisier F., Kiselev D., Mugnier Y., . Le Dantec R, Galez C., Wolf J.P. (2008). Nano-FROG: Frequency Resolved Optical Gating by a nanometric object. *Optics Express*, 16(14) 10405-10411

Extermann J., Bonacina L., Cuna E., Kasparian C., Mugnier Y., Feurer T., Wolf J.P. (2009). Nanodoublers as deep imaging markers for multi-photon microscopy. *Optics Express*, 17(17) 15342-15349

Fu D., Zhang Y., Liu J., Lu Z. (2001). Hyper-Rayleigh scattering of CdS nanoparticles stabilized by inorganic heteropolyanions. *Mater. Lett.* 51, 183-186

Galez C., Mugnier Y., Bouillot J., Lambert Y., and Le Dantec R. (2006). Synthesis and characterisation of Fe(IO3)3 nanosized powder. *J. Alloys Comp*. 416, 261-264

Hajj B., de Reguardati S., Hugonin L., Le Pioufle B., Osaki T., Suzuki H., Takeuchi S., Mojzisova H., Chauvat D., Zyss J. (2009). Electro-Optical Imaging Microscopy of Dye-Doped Artificial Lipidic Membranes *Biophys. J.* 97(11), L29

Hajj B., Gacoin T., Zyss J., Chauvat D. (submitted 2010). Electrooptical Pockels scattering from a single nanocrystal.

Halbout J.-M., Blit S., Chung T. (1984). Evaluation of the phase-matching properties of nonlinear optical materials in the powder form. *IEEE Journ. of Quant. El.* 17(4), 513-517

Hellwarth, R. Christensen, P. (1974). Nonlinear optical microscope examination of structures in polycrystalline ZnSe. *Opt. Commun*, 12, 318-322

Hsieh C. L., Grange R., Pu Y., and Psaltis D. (2009). Three-dimensional harmonic holographic microcopy using nanoparticles as probes for cell imaging. *Opt. Express* 17(4), 2880–2891

Hsieh C. L., Pu Y., Grange R., and Psaltis D. (2010). Digital phase conjugation of second harmonic radiation emitted by nanoparticles in turbid media. *Opt. Express* 18(12), 12283-12290

Hsieh C. L., Grange R., Pu Y., and Psaltis D. (2010). Bioconjugation of barium titanate nanocrystals with immunoglobulin G antibody for second harmonic radiation imaging probes. *Biomaterials* 31(8), 2272–2277

Johnson J. C., Yan H. Q., Schaller R. D., Petersen P. B., Yang P. D., and Saykally R. J. (2002). Near-field imaging of nonlinear optical mixing in single zinc oxide nanowires. Nano Lett. 2(4), 279–283

Josse D., Dou S.X., Zyss J., Andreaaza P., Périgaud A. (1992). Near-Infrared Optical parametric Oscillation in a N-(4-Nitrophenyl)-L-Prolinol Molecular Crystal. *Appl.Phys.Lett.* 61,121

Kachynski A. V., Kuzmin A. N., Nyk M., Roy I., and Prasad P. N. (2008). Zinc oxide nanocrystals for nonresonant nonlinear optical microscopy in biology and medicine. *J. Phys. Chem. C* 112(29), 10721–10724

Komorowska K., Brasselet S., Zyss J., Pourlsen L., Jazdzyk M., Egelhaaf H.J., Gierschner J., Hanack M. (2005). Nanometric scale investigation of the nonlinear efficiency of perhydrotriphynylene inclusion compounds. *Chem. Phys*. 318 (1-2), 12-20

Kuo T. R., Wu C. L., Hsu C. T., Lo W., Chiang S. J., Lin S. J., Dong C. Y., and Chen C. C., (2009). Chemical enhancer induced changes in the mechanisms of transdermal delivery of zinc oxide nanoparticles. *Biomaterials* 30(16), 3002–3008

Kurtz S. K., Perry T. T. (1968). A Powder Technique for the Evaluation of Nonlinear Optical Materials. *J. Appl. Phys*., 39, 3798–3813

Le X. L., Zhou C., Slablab A., Chauvat D., Tard C., Perruchas S., Gacoin T., Villeval P., and Roch J. F. (2008). Photostable second-harmonic generation from a single KTiOPO4 nanocrystal for nonlinear microscopy. *Small* 4(9), 1332–1336

Le X. L., Brasselet S., Treussart F., Roch J. F., Marquier F., Chauvat D., Perruchas S., Tard C., and Gacoin T. (2006). Balanced homodyne detection of second-harmonic generation from isolated subwavelength emitters. *Appl.Phys. Lett*. 89(12), 121118

Le Bozec, H., Le Bouder, T., Maury, O., Bondon, A., Ledoux, I., Deveau, S., Zyss, J (2001). Supramolecular Octupolar Self-organization towards Nonlinear Optics. *Adv. Mater.*, 13, 1677-1681

Le Floc'h V., Brasselet S., Roch J.F., Zyss J. (2003). Monitoring of orientation in molecular ensembles by polarization sensitive nonlinear microscopy. *J. Phys. Chem. B*, 107, 12403-12410

Le Floc'h V., Brasselet S., Zyss J., Chao R., Lee S.H., Jeon S.J., Cho M., Min K.S., Suh M.P. (2005). High efficiency and quadratic optical properties of a fully optimized 2D octupolar crystal by nonlinear microscopy. *Adv. Mater.* 17(2),196-200

Magrez, A. , et al. (2006). Growth of single-crystalline KNbO3 nanostructures. *J. Phys. Chem. B* 110, 58–61

Mugnier Y., Houf L., El-Kass M., Le Dantec R. , Hadji R., Vincent B., Djanta G., Badie L., Eschbach J., Rouxel D. and Galez C. (submitted 2010). In situ crystallization and growth dynamics of acentric iron iodate nanocrystals in w/o microemulsions probed by Hyper-Rayleigh Scattering measurements.

Nakayama Y., Pauzauskie P. J., Radenovic A., Onorato R. M., Saykally R. J., Liphardt J., and Yang P. D. (2007). Tunable nanowire nonlinear optical probe. *Nature* 447(7148), 1098–1101

Oudar J.L., Chemla D.S. (1977). Hyperpolarizabilities of the nitroanilines and their relations to the excited state dipole moment. *J. Chem. Phys* 66, 2664-2670

Pu Y., Centurion M., Psaltis D. (2008). Harmonic Holography–a new holographic principle. *Appl. Opt.* 47 A103-A110

Rekaï, E. D., Baudin, J. B., Jullien, L., Ledoux, I., Zyss, J., Blanchard-Desce, M. *Chem.Eur. J.* 2001, 7, 4395

Revillod G., Duboisset J., Russier-Antoine I., Benichou E., Bachelier G., Jonin Ch., Brevet P.F. (2008). Multipolar Contributions to the Second Harmonic Response from Mixed DiA-SDS Molecular Aggregates. *J. Phys. Chem*. C 112, 2716

Richards B., and Wolf E. (1959). Electromagnetic diffraction in optical systems. 2. Structure of the image field in an aplanatic system. *Proceedings of the Royal Society of London Series a-Mathematical and Physical Sciences* 253, 358–379

Rodríguez E. M., Speghini A., Piccinelli F., Nodari L., Bettinelli M., Jaque D., and Sole J. G. (2009). Multicolour second harmonic generation by strontium barium niobate nanoparticles. *J. Phys. D Appl. Phys.* 42(10), 4

Rodriguez E. V., de Araujo C. B., Brito-Silva A. M., Ivanenko V. I., and Lipovskii A. A. (2009), Hyper-Rayleigh scattering from BaTiO3 and PbTiO3 nanocrystals. *Chem. Phys. Lett.* 467(4-6), 335–338

Sandeau N., Le X.L. , Chauvat D., Zhou C., Roch J. F., and Brasselet S. (2007). Defocused imaging of second harmonic generation from a single nanocrystal. *Opt. Express* 15(24), 16051–16060

Sanz N., Baldeck P. L., Nicoud J. F., LeFur Y., and Ibanez A. (2001), Solid State Sci. 3, 867.

Shen Y., Swiatkiewicz J., Winiarz J., Markowicz P., Prasad P. (2000), Second-harmonic and sum-frequency imaging of organic nanocrystals with photon scanning tunneling microscope. *Appl.Phys.Lett.* 77, 2946 (2000)

Schön P., Munhoz F., Gasecka A., Brustlein S., and Brasselet S. (2008). Polarization distortion effects in polarimetric two-photon microscopy. *Opt. Express* 16(25), 20891–20901

Schön P., Behrndt M., Ait-Belkacem D., Rigneault H., Brasselet S. (2010). Polarization and Phase Pulse Shaping applied to Structural Contrast in Nonlinear Microscopy Imaging. *Phys. Rev. A* 81, 013809

Terhune R.W., Maker P.D., SavageC.M. (1965). Measurements of Nonlinear Light Scattering. *Phys. Rev. Lett.* 14, 681-684.

Toury T., Brasselet S., Zyss J. (2006) Electro-optical microscopy: mapping nonlinear polymer films with micrometric resolution *Opt. Lett.* 31(10), 1468-1470

Trebino R., DeLong K.W., Fittinghoff D.N., Sweetser J.N., Krumbügel M.A., Richman B.A., and Kane D.J. (1997). Measuring ultrashort laser pulses in the time-frequency domain using frequency-resolved optical gating. *Rev. Sci. Instrum.* 68, 3277

Treussart F., Botzung-Appert E., Ha-Duong N.-T., Ibanez , Roch J.-F., Pansu R. (2003). Second Harmonic Generation and Fluorescence of CMONS Dye Nanocrystals Grown in a Sol-Gel Thin Film. *ChemPhysChem* 4, 757–760

Wang X., Zhang Y., Wang G., Zhang C., Fu D., Shen Y., Lu Z., Cui Y., Ochiai S., Uchida Y., Kojima K. and Ohashi A. Second-order nonlinear optical properties of centrosymmetric nanoparticles studied by hyper-Rayleigh scattering (HRS) technique. (2005). *Chinese Optics Letters*, Vol. 3, Issue S1, S125-S127

Wnuk P., Le L. X., Slablab A., Tard C., Perruchas S., Gacoin T., Roch J. F., Chauvat D., and Radzewicz C. (2009). Coherent nonlinear emission from a single KTP nanoparticle with broadband femtosecond pulses. *Opt. Express* 17(6), 4652–4658

Yew E. Y. S., and Sheppard C. J. R. (2006). Effects of axial field components on second harmonic generation microscopy. *Opt. Express* 14(3), 1167–1174

Yi T., Tancrez N., Clément R., Ledoux-Rak I., Zyss J. (2004). Organic-MPS3 nanocomposites with large second-order nonlinear optical response. *J. Lumin*, 110, 389-395

Yi T., Clément R., Haut C., Catala L., Gacoin T., Tancrez N., Ledoux I., Zyss J. (2005). J-Aggregated Dye-MnPS3 Hybrid Nanoparticles with Giant Quadratic Optical Nonlinearity. *Adv. Mater.* 17, 335-338

Yokoyama, S., Nakahama, T., Otomo, A., Mashiko, S (2000). Enhancement of the Molecular Hyperpolarizability in Multi-choromophoric Dipolar Dendrons. *J. Am. Chem. Soc.*, 122, 3174-3181

Zielinski M., Oron D., Chauvat D., and Zyss J. (2009). Second-harmonic generation from a single core/shell quantum dot. *Small* 5(24), 2835–2840

Zyss J. and Oudar J.L. (1982). Relations between microscopic and macroscopic lowest order optical nonlinearities of molecular crystals in one and two-dimensional units. *Phys Rev A* 26 (4), 2028-2048

Zyss J., Nicoud J.F., Coquillay M. (1984). Chirality and hydrogen-bonding in molecular crystals for phase-matched second-harmonic generation: N-(4-nitrophenyl)-(L)-prolinol (NPP). *J. Chem. Phys.* 81, 4160

Zyss J. and Ledoux I. (1994) Nonlinear Optics in Multipolar Media: Theory and Experiments. *Chem.Rev.*94,77-105

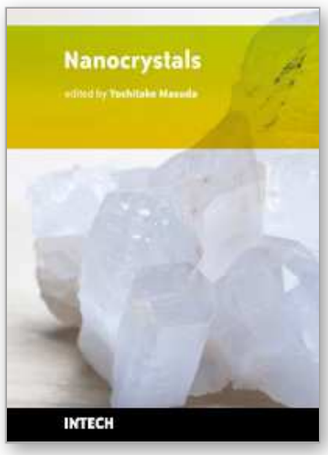

Nanocrystals

Edited by Yoshitake Masuda

ISBN 978-953-307-126-8
Hard cover, 326 pages
Publisher Sciyo
Published online 06, October, 2010
Published in print edition October, 2010

This book contains a number of latest research developments on nanocrystals. It is a promising new research area that has received a lot of attention in recent years. Here you will find interesting reports on cutting-edge science and technology related to synthesis, morphology control, self-assembly and application of nanocrystals. I hope that the book will lead to systematization of nanocrystal science, creation of new nanocrystal research field and further promotion of nanocrystal technology for the bright future of our children.

How to reference

In order to correctly reference this scholarly work, feel free to copy and paste the following:

Sophie Brasselet and Joseph Zyss (2010). Nano-Crystals for Quadratic Nonlinear Imaging : Characterization and Applications, Nanocrystals, Yoshitake Masuda (Ed.), ISBN: 978-953-307-126-8, InTech, Available from: http://www.intechopen.com/books/nanocrystals/nano-crystals-for-quadratic-nonlinear-imaging-characterization-and-applications

INTECH
open science | open minds

InTech Europe
University Campus STeP Ri
Slavka Krautzeka 83/A
51000 Rijeka, Croatia
Phone: +385 (51) 770 447
Fax: +385 (51) 686 166
www.intechopen.com

InTech China
Unit 405, Office Block, Hotel Equatorial Shanghai
No.65, Yan An Road (West), Shanghai, 200040, China
中国上海市延安西路65号上海国际贵都大饭店办公楼405单元
Phone: +86-21-62489820
Fax: +86-21-62489821

IntechOpen